

Reference frame transformation of satellite gravity gradients and topographic mass reduction

Johannes Bouman,¹ Jörg Ebbing,² and Martin Fuchs¹

Received 5 September 2012; revised 20 November 2012; accepted 21 November 2012; published 28 February 2013.

[1] The Gravity field and steady state Ocean Circulation Explorer (GOCE) is the European Space Agency's mission that combines GPS tracking and gravity gradiometry to determine the Earth's mean gravity field with unprecedented, global accuracy with a spatial resolution down to 80 km. This resolution makes GOCE gravity gradient data in particular useful for lithospheric scale modeling. However, the relation between coordinates in a model frame and at satellite altitude is not straightforward, and most geophysical modeling programs require a planar approximation, which may not be appropriate for satellite data. We derive the exact relation between the model reference frame, in which gradients from lithospheric modeling are given, and the local north-oriented frame in which GOCE gradients at 255 km altitude are given. We generated gradients from a GOCE gravity field model and assessed whether the orientation differences between local north-oriented frame and model reference frame are relevant. In addition, we assessed the same for airborne gradiometry at an altitude of 5 km because these data are complementary to GOCE. We find that if the regional area has a longitude extension of 5°, the errors stay below 10%. For larger areas the standard deviation of the systematic errors may be 40% of the signal standard deviation. Comparing topographic mass reduction in planar and spherical approximation, one sees significant long wavelength differences in terms of gravity gradients or gradient-tensor invariants. The maximum error is up to 1 E at satellite altitude compared with maximum signal amplitude of 3 E. Planar approximation is therefore not accurate enough for topographic mass reduction of GOCE gravity gradients.

Citation: Bouman, J., J. Ebbing, and M. Fuchs (2013), Reference frame transformation of satellite gravity gradients and topographic mass reduction, *J. Geophys. Res. Solid Earth*, 118, 759–774, doi:10.1029/2012JB009747.

1. Introduction

[2] Regional models of the Earth's lithosphere are frequently setup in planar approximation using Cartesian coordinates. Specifically, the universal transverse mercator (UTM) projection is commonly used for the horizontal coordinates, and heights and depths are given with respect to the associated plane. The regional models are usually based on seismic and/or magnetic and gravitational potential data acquired on or close to the Earth's surface [e.g., Zeyen and Fernández, 1994; Tašárová et al., 2006; Popowski et al., 2009; Barrère et al., 2011]. Because of the limited height of data acquisition, and as long as the extension of the study area is limited, planar approximation may be sufficient and the relation between the model reference frame (MRF) and measurement reference

frame is straightforward. In March 2009, however, the Gravity field and steady state Ocean Circulation Explorer (GOCE) satellite was launched, which gravitational gradient measurements have found application in lithospheric modeling [Bouman et al., 2011a; Braatenberg et al., 2011; Álvarez et al., 2012; Hirt et al., 2012]. Because of the height of the satellite—GOCE has a perigee height of 255 km above the Earth's surface—planar approximation may no longer be adequate.

[3] The GOCE observed gradients are given in geocentric coordinates, which can easily be referred to the reference ellipsoid because the transformation from spherical coordinates to ellipsoidal coordinates is straightforward. The MRF commonly uses the UTM-projection, which is a transversal cylindrical projection and at the central meridian the ellipsoid and cylinder coincide. Also, the relation between the ellipsoid and the plane is known, at least when the height is zero. For GOCE gradients at satellite altitude the height is obviously not zero and the exact relation needs to be derived. With respect to the vertical direction the ellipsoidal normal coincides with the planar normal for the central meridian. For other meridians there is an angle between the ellipsoidal and planar normal. In the plane the x -axis points east (easting), the z -axis is along the normal and the y -axis points north (northing).

¹Deutsches Geodätisches Forschungsinstitut (DGFI), Munich, Germany.

²Geological Survey of Norway (NGU), Trondheim, Norway.

Corresponding author: J. Bouman, Deutsches Geodätisches Forschungsinstitut (DGFI), Alfons-Goppel-Str. 11, D-80539 Munich, Germany. (bouman@dgfi.badw.de)

©2012. American Geophysical Union. All Rights Reserved.
2169-9313/13/2012JB009747

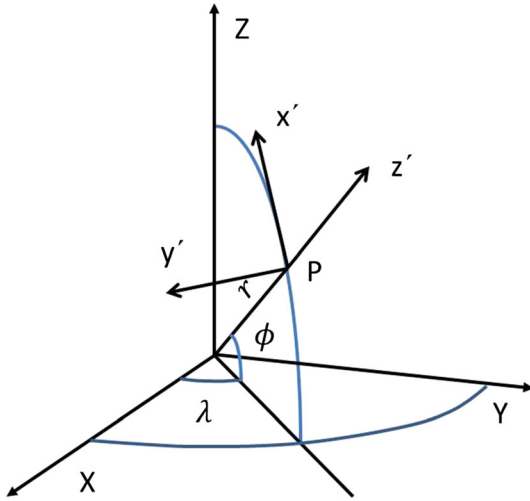


Figure 1. Geocentric Cartesian, local north-oriented and geocentric spherical coordinates systems.

Also, map north and east in the plane do not coincide with geographical north and east of the ellipsoid except for the central meridian. In addition, it is not directly clear how to connect the planar Cartesian frame from a UTM projection to spherical or ellipsoidal coordinates at satellite altitude.

[4] In this paper, we will derive the relation between UTM coordinates and associated height, and their geocentric counterparts, as well as the relation between the orientation in the model and measurement reference frames. The reference frames are defined in section 2 and the relations between coordinates and orientations are derived in section 3. The relations are illustrated by examples derived from GOCE gravity field models as well as synthetic airborne gradiometer data. Section 4 addresses the validity of planar versus spherical approximation as far as topographic reductions are concerned.

2. Reference Frame Definitions

[5] The model reference frame, derived from the UTM projection, and the satellite measurement reference frame are defined in this section.

2.1. Geocentric and Geographic Coordinates

[6] Geocentric spherical coordinates (r, ϕ, λ) are used for a sphere whereas geographic (or geodetic) coordinates (h, φ, λ) are used for the ellipsoid. The longitude λ is the same in both coordinate systems, whereas geodetic and geocentric latitude differ. The height above the ellipsoid is h and the radial distance is r . The relation between geodetic latitude φ and geocentric latitude ϕ is

$$\tan \phi = (1 - e^2) \tan \varphi, \quad (1)$$

with e the first eccentricity [Torge, 2001]. The relation between the geographic and geocentric spherical coordinates on the one hand and geocentric Cartesian coordinates (X, Y, Z) are given in Appendix A. In the Earth-centered Earth-fixed (ECEF) system (X, Y, Z) the X -axis points to Greenwich and the Z -axis to the North Pole, see Figure 1.

2.2. Measurement Reference Frame

[7] The gradiometer reference frame (GRF) is a measurement reference frame and it is the coordinate system in which the gravity gradients are measured by GOCE. The GRF represents the reference for the positioning and orientation of the whole instrument with respect to external reference frames. Details are specified in Gruber et al. [2010]. The GOCE quaternions relate the GRF to the inertial reference frame, which in turn allows relating the gradients to the ECEF reference frame that corotates with the Earth.

[8] The local north-oriented frame (LNOF) is a right-handed north-west-up frame with the X -axis pointing north, the Y -axis pointing west, and the Z -axis pointing up. Besides the GRF, the GOCE calibrated gravity gradients are provided also in the LNOF [Bouman et al., 2009, 2011b; Fuchs and Bouman, 2011]. The LNOF is defined as follows:

[9] 1. The origin is located at the actual (or nominal) satellite center of mass

[10] 2. z' is defined as the vector from the geocenter to the origin, pointing radially outward,

[11] 3. y' is parallel to the normal vector to the plane of the geocentric meridian of the satellite center of mass, pointing westward,

[12] 4. x' is parallel to the normal vector to the plane defined by y' and z' and forms a right-handed system.

[13] The LNOF is a local Cartesian system that is defined with respect to spherical coordinates. The ECEF and the LNOF are related as follows, see Figure 1:

$$\begin{pmatrix} X \\ Y \\ Z \end{pmatrix} = \begin{pmatrix} -\cos \lambda \sin \phi & \sin \lambda & \cos \lambda \cos \phi \\ -\sin \lambda \sin \phi & -\cos \lambda & \sin \lambda \cos \phi \\ \cos \phi & 0 & \sin \phi \end{pmatrix} \begin{pmatrix} x' \\ y' \\ z' + r \end{pmatrix}. \quad (2)$$

2.3. Model Reference Frame

[14] The UTM projection is a conformal mapping of the Earth ellipsoid. It uses a two-dimensional Cartesian coordinate system (x, y) to identify locations on the Earth independently of the vertical position. The system divides the Earth into 60 zones, within each zone a central meridian λ_0 that is mapped into a straight line at constant scale. UTM is a cylindrical projection with the axis of the cylinder in the equatorial plane (see Figure 2). The forward and inverse mapping between geographic longitude λ and latitude φ to UTM are given in Appendix A. These mappings have errors smaller than $0.3 \mu\text{m}$ within 1000 km of the central meridian [Krüger, 1912; Karney, 2011]. The coordinates in the rotated ECEF are denoted as (X', Y', Z') where this frame is rotated over an angle λ_0 around the Z -axis with respect to the ECEF.

[15] Because of meridian convergence the map north and geographic north differ. The angle between the true north and the projected north is given by [Strang van Hees, 2006]

$$\gamma = \Delta \lambda \sin \varphi + \frac{\Delta \lambda^3}{3} \sin \varphi \cos^2 \varphi \left(1 + 3n'^2 + 3n'^4 \right) + \frac{\Delta \lambda^5}{15} \sin \varphi \cos^4 \varphi (2 - \tan^2 \varphi), \quad (3)$$

with $\Delta \lambda = \lambda - \lambda_0$ the longitude difference between the central meridian and the computation point, and $n' = \frac{e^2 \cos^2 \varphi}{1 - e^2}$.

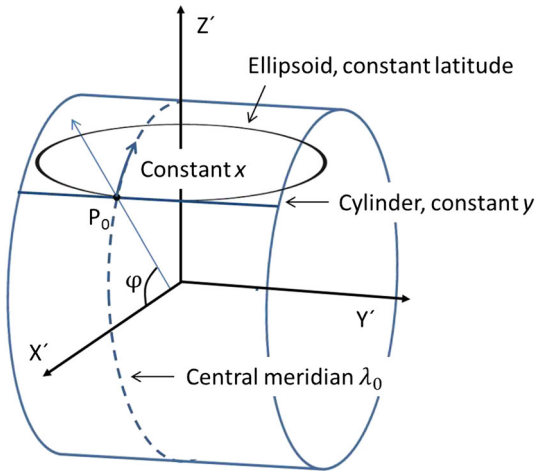


Figure 2. Transversal cylinder, rotated ECEF reference frame (X' , Y' , Z') and central meridian, and one parallel of the ellipsoid.

[16] Although the UTM projection defines horizontal locations only, in regional models heights are associated with the planar coordinates. Because the normal to ellipsoid and the normal to the cylinder differ in general, not only the map north and geographic north differ, but also map up-down and geographic up-down. This is illustrated in Figure 3, which displays the same parallel at constant latitude φ as Figure 2. How to account for these orientation differences is discussed in the next section.

3. From Measurement to Model Reference Frame and Vice Versa

[17] The exact coordinate transformation between ECEF and MRF is derived first, after which the rotation from the LNOF—where measured gradients are given—to the MRF is discussed. Examples from GOCE gradiometry and airborne gradiometry serve as illustration.

3.1. Coordinate Transformation

[18] The transformation of the planar coordinates $(x, y, z=0)$ to geographic coordinates $(\varphi, \lambda, h=0)$ is straightforward. Now the question is how to relate arbitrary (x, y, z) coordinates to

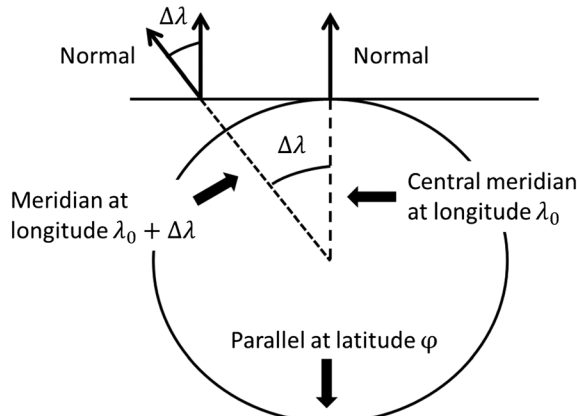


Figure 3. Normal to ellipsoid and cylinder at a constant latitude.

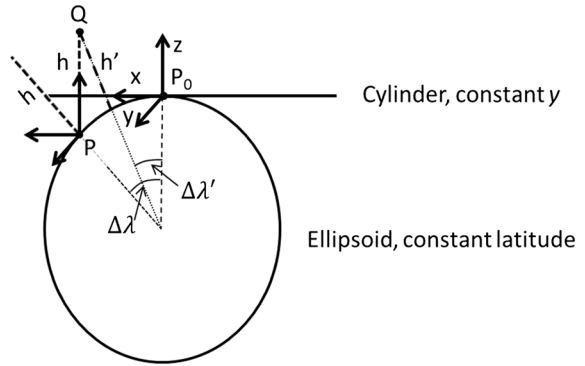


Figure 4. Cylindrical normal direction at ellipsoid and ellipsoidal normal direction at height h .

(φ, λ, h) . Because the cylindrical and ellipsoidal normal differ, a height h along the cylindrical normal will differ from a height h along the ellipsoidal normal, which is shown in Figure 4, where it should be noted that the reference surface remains the ellipsoid. In first approximation, the planar or cylindrical normal equals the ellipsoidal, but this is not exactly true except for the central meridian. In fact, also the geographic latitude and longitude change when $z \neq 0$. If we want to relate gravity anomalies or gravity gradients from regional geophysical models to measurements at altitude, we need to relate planar coordinates $(x, y, z=h)$ to geographic coordinates (φ, λ, h') or geocentric Cartesian coordinates (X, Y, Z) .

3.1.1. Forward Transformation: MRF to ECEF

[19] Suppose we have a point P on the ellipsoid with geographic coordinates $(\varphi, \lambda, 0)$ and easting and northing (x, y) (see Figure 4). We are now looking for the geographic coordinates of point Q with coordinates $(x, y, z=h)$. The idea is to use two properties: (1) the ellipsoidal normal and cylindrical normal are equal at the central meridian; (2) for constant y and variable x the cylindrical normal direction does not change (see also Figure 2). If one therefore computes the coordinate differences $(\Delta X, \Delta Y, \Delta Z)$ in the ECEF for the central meridian along the cylindrical normal, then one can add these differences to the geocentric Cartesian coordinates of P to obtain the geocentric Cartesian coordinates of Q . From the latter geographic or spherical coordinates can be derived.

[20] Given is point P with coordinates $(x, y, z=0)$. The steps to compute the ECEF coordinates of point Q are as follows:

[21] 1. For the (x, y) -pair of P compute the corresponding (x_0, y_0) -pair at the central meridian (point P_0)

[22] 2. Compute ellipsoidal coordinates (φ_0, λ_0) from (x_0, y_0) ; see Appendix A

[23] 3. Convert ellipsoidal coordinates $(\varphi_0, \lambda_0, 0)$ and $(\varphi_0, \lambda_0, h)$ to (X_0, Y_0, Z_0) and (X_h, Y_h, Z_h) ; see Appendix A

[24] 4. Compute coordinate difference $(\Delta X, \Delta Y, \Delta Z) = (X_h, Y_h, Z_h) - (X_0, Y_0, Z_0)$

[25] 5. Compute ellipsoidal coordinates (φ, λ) from (x, y) of point P

[26] 6. Convert ellipsoidal coordinates $(\varphi, \lambda, 0)$ of P to (X, Y, Z) and add $(\Delta X, \Delta Y, \Delta Z)$; these are the Cartesian coordinates in the ECEF frame of point Q

3.1.2. Inverse Transformation: ECEF to MRF

[27] For the transformation from ECEF to MRF one may use an iterative procedure. Because the geographic latitude and longitude of Q and P are different, the corresponding

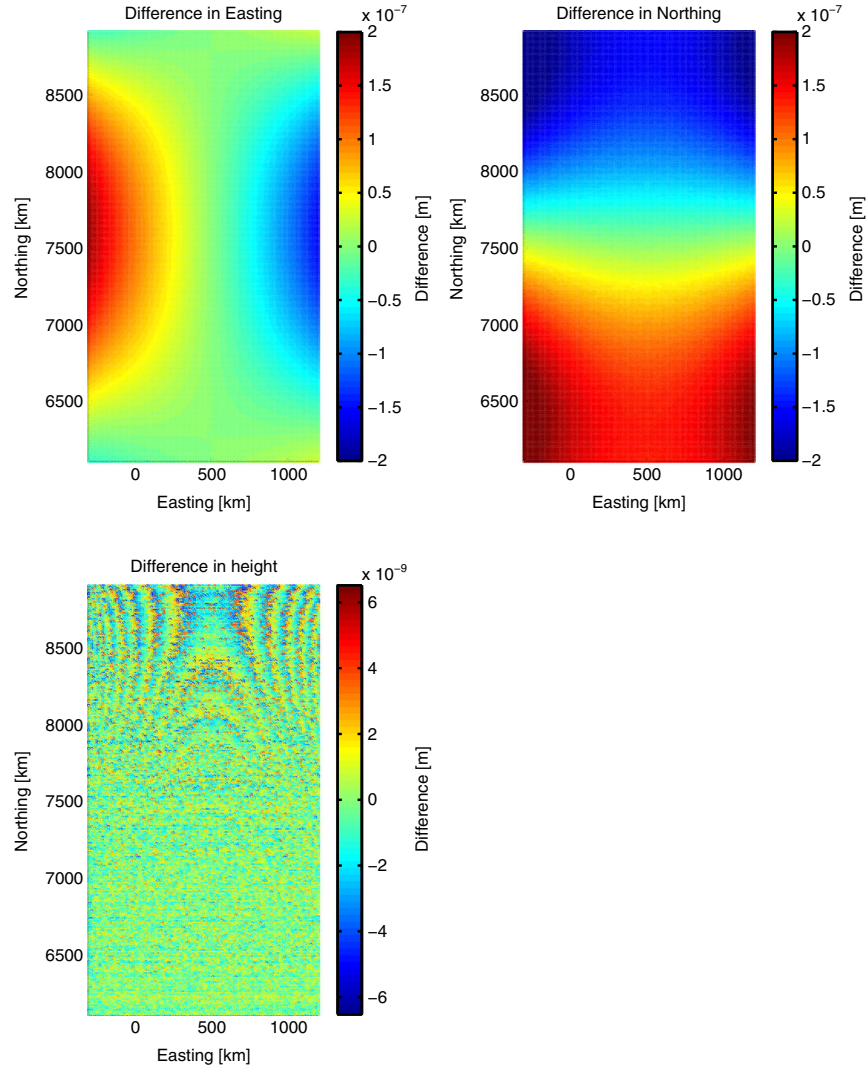


Figure 5. Differences in easting, northing, and height in [m] after forward and inverse transformation.

northing and easting are different as well. Consequently, one cannot directly compute the northing and easting of point P_0 starting from Q . Suppose the geocentric Cartesian coordinates of Q are given. Then

[28] 1. Convert Cartesian coordinates (X, Y, Z) to geodetic coordinates (φ, λ, h)

[29] 2. Use these ellipsoidal coordinates with $h=0$ to compute $(x, y)_i$

[30] 3. For a $(x, y)_i$ -pair compute the corresponding $(x_0, y)_i$ -pair at the central meridian (point P_0)

[31] 4. Compute ellipsoidal coordinates $(\varphi_0, \lambda_0)_i$ from $(x_0, y)_i$

[32] 5. Convert ellipsoidal coordinates $(\varphi_0, \lambda_0, 0)_i$ and $(\varphi_0, \lambda_0, h)_i$ to $(X_0, Y_0, Z_0)_i$ and $(X_h, Y_h, Z_h)_i$

[33] 6. Compute coordinate differences $(\Delta X, \Delta Y, \Delta Z)_i = (X_h, Y_h, Z_h)_i - (X_0, Y_0, Z_0)_i$

[34] 7. Reduce coordinates with updated height estimate (this is the height reduction in the direction of the cylindrical normal):

$$\begin{bmatrix} dX \\ dY \\ dZ \end{bmatrix}_i = \begin{bmatrix} X \\ Y \\ Z \end{bmatrix} - \begin{bmatrix} \Delta X \\ \Delta Y \\ \Delta Z \end{bmatrix}_i,$$

[35] 8. Convert reduced Cartesian coordinates to ellipsoidal coordinates $(\varphi, \lambda, dh)_i$; dh should be zero after convergence; If $dh_i > \epsilon$ then $h_{i+1} = h_i + dh_i$ and $i = i + 1$ and go to 2.

3.1.3. Example

[36] We use a region in the North East Atlantic (NEA) to test our algorithms. The corresponding UTM zone is 33 N, but we use an extended zone. The corresponding geographic coordinates vary from about 50 to 80° latitude and –20 to 40° longitude. If we use the above procedure for forward and inverse transformation and subtract coordinates $(x, y, z = h)$ before and after transformation, then we get the coordinate differences shown in Figure 5. As input a height above the plane of 255 km has been used. All differences are below 1 μm, which is quite sufficient for our purposes, that is, lithospheric modeling.

[37] If we use the above procedure for forward transformation then we get for heights above the ellipsoid for the NEA the values shown in Figure 6 (left panel). As input a height above the plane of 255 km has been used. The maximum difference is less than 2 km in this case. To assess whether the height difference matters when comparing the geophysical model with GOCE measured gradients, we

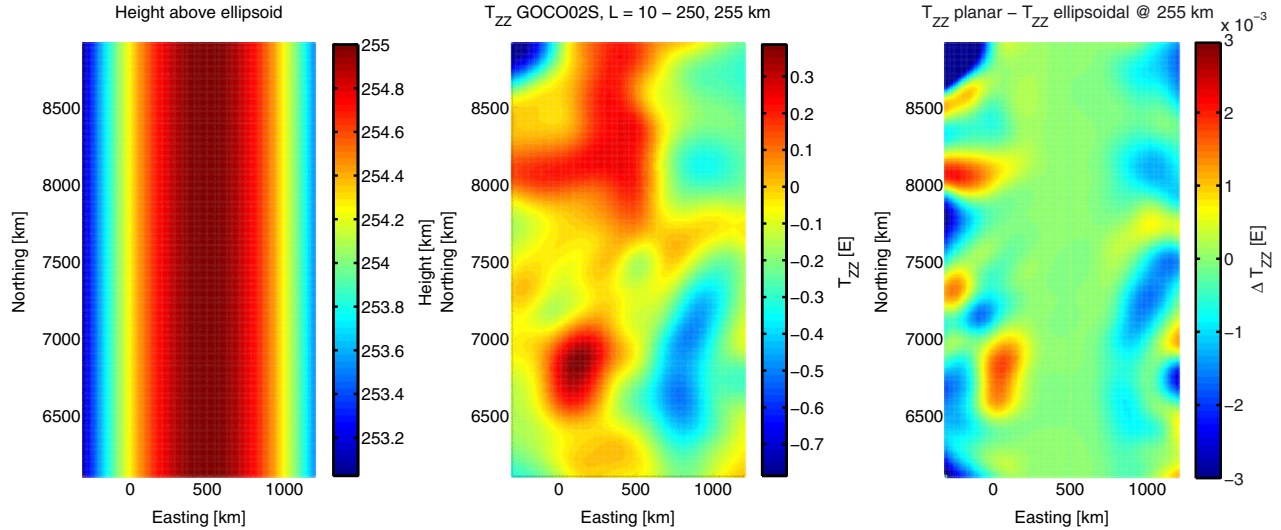


Figure 6. (left) Height above ellipsoid starting from a height above the plane of 255 km. (middle) Vertical gravity gradient at 255 km above ellipsoid in E using GOCO02S, $L = 10 - 250$. (right) Difference in vertical gravity gradient in E computed at height above ellipsoid from the left panel and exactly 255 km; color bar saturated to ± 3 mE.

computed vertical gravity gradients from GOCO02S using spherical harmonic degree $L = 10 - 250$ [Goiginger *et al.*, 2011]. The ultralong wavelengths for spherical harmonic degrees $L < 10$ have been removed because they correspond to wavelengths larger than our study area and the corresponding gravity gradient signal is very smooth. These wavelengths usually are associated with the sublithospheric density structure of the Earth [e.g., Bowin, 1991]. The gradients for degree $L = 10 - 250$ are shown in the middle panel of Figure 6. We also computed the vertical gravity gradients at the heights between 253 and 255 km shown in the left panel of Figure 6, which corresponds to a planar height of 255 km. The differences between the two sets of gradients are shown in the right panel in Figure 6. Note the normal direction was taken equal for both sets. The statistics of the differences are shown in Table 1. The standard deviation of the differences is 1 mE, whereas the absolute maximum difference is about 12 mE. We therefore conclude that one may neglect the difference in planar and ellipsoidal height for our purposes.

3.2. Frame Rotation

3.2.1. Local North-Oriented Frame to Model Reference Frame

[38] GOCE gravity gradients are given in the GRF and the LNOF. Also airborne gravity gradients are given in an instrument frame, which can be related to the LNOF using

Table 1. Statistics of Differences [mE] Between Vertical Gravity Gradients at 255 km Above the Ellipsoid and 255 km Above the Plane

	T_{zz}
Standard deviation	1.0
Mean	-0.2
Maximum	2.2
Minimum	-12.3

geographic coordinates of the plane that are usually determined with GPS [e.g., Dransfield and Lee, 2004]. The relation between the LNOF and the ECEF is given in section 2.2. Here we will derive the relation between the MRF and the ECEF, which then connects the MRF to the LNOF.

[39] It will be convenient to introduce the rotated ECEF where the rotation is around the Z-axis such that the rotated X-axis points to the central meridian. If we rotate the X-axis to the central meridian we get the X' -system and we have

$$\begin{pmatrix} X' \\ Y' \\ Z' \end{pmatrix} = \begin{pmatrix} \cos \lambda_0 & \sin \lambda_0 & 0 \\ -\sin \lambda_0 & \cos \lambda_0 & 0 \\ 0 & 0 & 1 \end{pmatrix} \begin{pmatrix} X \\ Y \\ Z \end{pmatrix}. \quad (4)$$

[40] In this X' -system we consider the transverse cylinder with cylindrical coordinates (ρ, θ, x) . The relation between cylindrical coordinates and the X' -system is (see Figure 7),

$$\begin{aligned} X' &= \rho \cos \theta \\ Y' &= x + Y_p \\ Z' &= \rho \sin \theta \end{aligned} \quad (5)$$

with Y_p the Y -coordinate of the origin of the x -system in the rotated ECEF, and

$$\begin{aligned} \rho &= \sqrt{X'^2 + Z'^2} \\ \theta &= \text{atan} \frac{Z'}{X'} \end{aligned} \quad (6)$$

[41] It should be noted that by introducing these cylindrical coordinates and using the connection above to the rotated ECEF, we implicitly set the spherical normal equal to the ellipsoidal normal. Because the difference between ϕ and φ is less than 0.2° , the associated error in the gradients is small and will be neglected here.

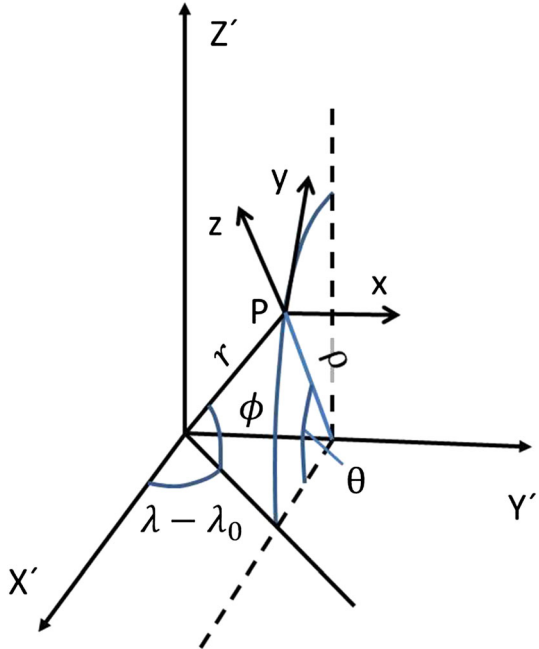


Figure 7. Rotated geocentric Cartesian, local cylindrical north-oriented, and geocentric spherical coordinates systems.

[42] The relation between the X' -system and the x -system (easting, northing, height) is

$$\begin{pmatrix} x \\ y \\ z \end{pmatrix} = R_1(90 - \theta)R_3(90) \begin{pmatrix} X' - X'_p \\ Y' - Y'_p \\ Z' - Z'_p \end{pmatrix} = \begin{pmatrix} 0 & 1 & 0 \\ -\cos(90 - \theta) & 0 & \sin(90 - \theta) \\ \sin(90 - \theta) & 0 & \cos(90 - \theta) \end{pmatrix} \begin{pmatrix} X' - X'_p \\ Y' - Y'_p \\ Z' - Z'_p \end{pmatrix}, \quad (7)$$

with X'_p, Y'_p, Z'_p the coordinates of the origin of the x -system in the rotated ECEF.

[43] Finally, the rotation from the x' -system (LNOF) to the x -system (MRF) is given as

$$\begin{pmatrix} x \\ y \\ z \end{pmatrix} = \begin{pmatrix} 0 & 1 & 0 \\ -c(90 - \theta) & 0 & s(90 - \theta) \\ s(90 - \theta) & 0 & c(90 - \theta) \end{pmatrix} \begin{pmatrix} c\lambda_0 & s\lambda_0 & 0 \\ -s\lambda_0 & c\lambda_0 & 0 \\ 0 & 0 & 1 \end{pmatrix} \begin{pmatrix} -c\lambda s\phi & s\lambda & c\lambda c\phi \\ -s\lambda s\phi & -c\lambda & s\lambda c\phi \\ c\phi & 0 & s\phi \end{pmatrix} \begin{pmatrix} x' \\ y' \\ z' \end{pmatrix}, \quad (8)$$

where sin and cos have been abbreviated as s and c , respectively.

[44] If we denote the total rotation as R_{tot} then the gravity gradients V'_{ij} transform as

$$V_{ij} = R_{\text{tot}} V'_{ij} R_{\text{tot}}^T, \quad (9)$$

and the inverse transformation is

$$V'_{ij} = R_{\text{tot}}^T V_{ij} R_{\text{tot}}. \quad (10)$$

[45] The procedure for the LNOF to MRF rotation now is

- [46] 1. Compute X -coordinates from spherical coordinates
- [47] 2. Compute X' -coordinates using the central meridian

[48] 3. Compute θ from X' and Z'

[49] 4. Compute the rotation matrix R_{tot} using the angles θ, ϕ, λ , and λ_0

[50] 5. Rotate.

3.2.2. Gravity Field and Steady State Ocean Circulation Explorer

[51] We want to assess whether one needs to account for the full LNOF to MRF rotation or that it may be sufficient to just correct for meridian convergence. We start with gravity gradients in the LNOF. At GOCE altitude (255 km in this case) gravity gradients were generated in a Cartesian grid using the GOCO02S global gravity field model from spherical harmonic degree 10–250. Figure 8 shows these gradients with x' north, y' west and z' up. In Figures 8–11, the top row contains the T_{xx} and T_{xy} gradients, the middle row the T_{xz} and T_{yy} gradients, and the bottom row the T_{yz} and T_{zz} gradients. The notation T_{ij} indicates that reduced instead of full gravity gradients V_{ij} are used. Next the gradient tensor was rotated to the MRF using the algorithms in section 3.2.1. Figure 9 shows the gradients after rotation to the MRF. Note that now x is easting and y is northing.

[52] Figure 10 shows the differences between the gradients in the MRF using the full rotation and gradients in the MRF accounting only for the difference in axes. That is, no corrections for meridian convergence or other corrections were applied. The statistics of the differences between full rotation and the approximation are summarized in Table 2. The maximum error is up to 0.2 E, which is large compared with the signal amplitude.

[53] Figure 11 shows the differences between the gradients in the MRF using the full rotation and gradients in the MRF accounting only for the meridian convergence. The statistics of the differences between full rotation and the approximation are summarized in Table 3. The maximum error is up to 0.1 E or so, which is still large compared with the signal. Especially the error in the T_{yy} component was reduced. Note that the rotation is around the z -axis and the statistics for the T_{zz} component did not change with respect to the previous case.

[54] We therefore conclude that it is not sufficient to correct only for meridian convergence. If gradients in MRF and LNOF are to be compared, applying a full rotation is required.

3.2.3. Airborne Gradiometry

[55] We have seen that at satellite altitude the difference in map north and geographic north as well as the difference between cylindrical and spherical (or ellipsoidal) normal needs to be taken into account when using GOCE gravity gradients for lithospheric modeling. Here we address whether these orientation differences are also relevant at much lower altitudes and we study airborne gradiometry. Similar to the GOCE case we rely on synthetic gravity gradients. For GOCE we used the global gravity field model GOCO02S with a maximum spherical harmonic degree of 250, which corresponds to a spatial resolution at the Earth's of about 80 km. Although such a resolution is adequate at satellite altitude, it is not when studying airborne gradiometry. We therefore use the high resolution global gravity field model EGM2008 with a maximum spherical harmonic degree of 2190 [Pavlis *et al.*, 2012], which corresponds to a spatial resolution at the Earth's surface of about 10 km. Gravity gradients were generated at a height of 5 km using EGM2008 with

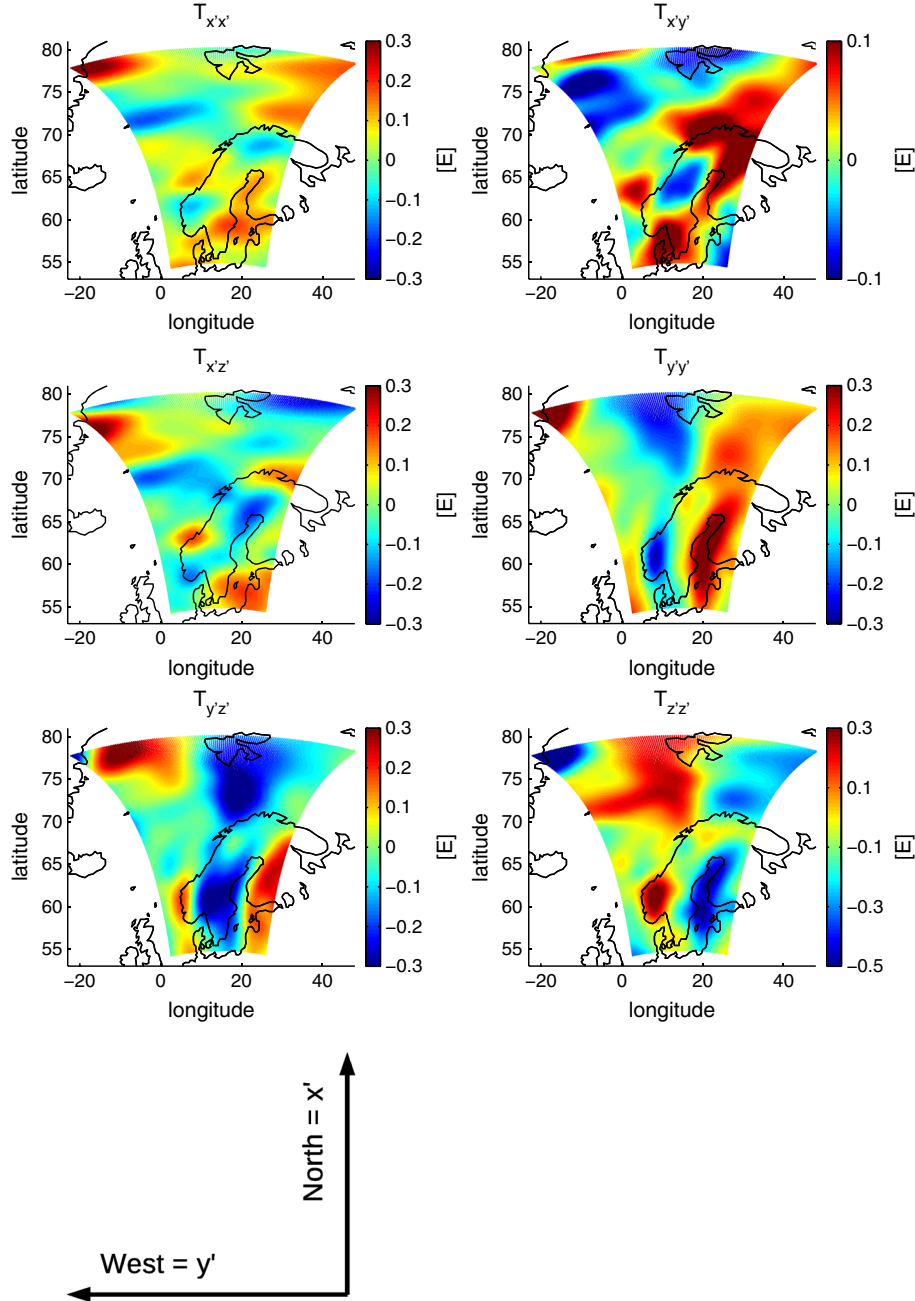


Figure 8. Gravity gradients in LNOF at GOCE altitude computed from GOCO02S degree 10–250. Color scales have been saturated. Note that x' is north and y' is west.

spherical harmonic degree 10–2190. The gradients were generated in the LNOF and the corresponding signal for T_{xy} and T_{zz} is shown in Figure 12. The gradients are correlated with the topography and bathymetry, as could be expected. The statistics of the gradients are summarized in Table 4, and we see that the standard deviation varies from 7 E for T_{xy} to 20 E for T_{zz} .

[56] Figure 13 shows the differences between gradients in the MRF using the exact rotation derived in section 3.2.1 and gradients in the MRF derived from the LNOF ignoring the orientation differences. The statistics of the differences are summarized in Table 5. Close to the central meridian with $\lambda = 15^\circ$ the errors are small, but they rapidly increase

with longitude. For the whole region, the standard deviation of the errors is 2.1–3.4 E or 10–40% of the signal standard deviation.

[57] In order to assess to what extent the orientation differences are acceptable, we computed the relative gravity gradient error in bands within 5, 10, and 15° from the central meridian (so the bands are 10, 20, and 30° respectively). These errors are shown in Table 6, and for comparison the relative error for the whole area is repeated. One therefore sees that if the error has to stay below 10% for example, then one has to stay within 5 degree of the central meridian. Otherwise full rotation should be done. We thus conclude that the difference LNOF – MRF is also relevant

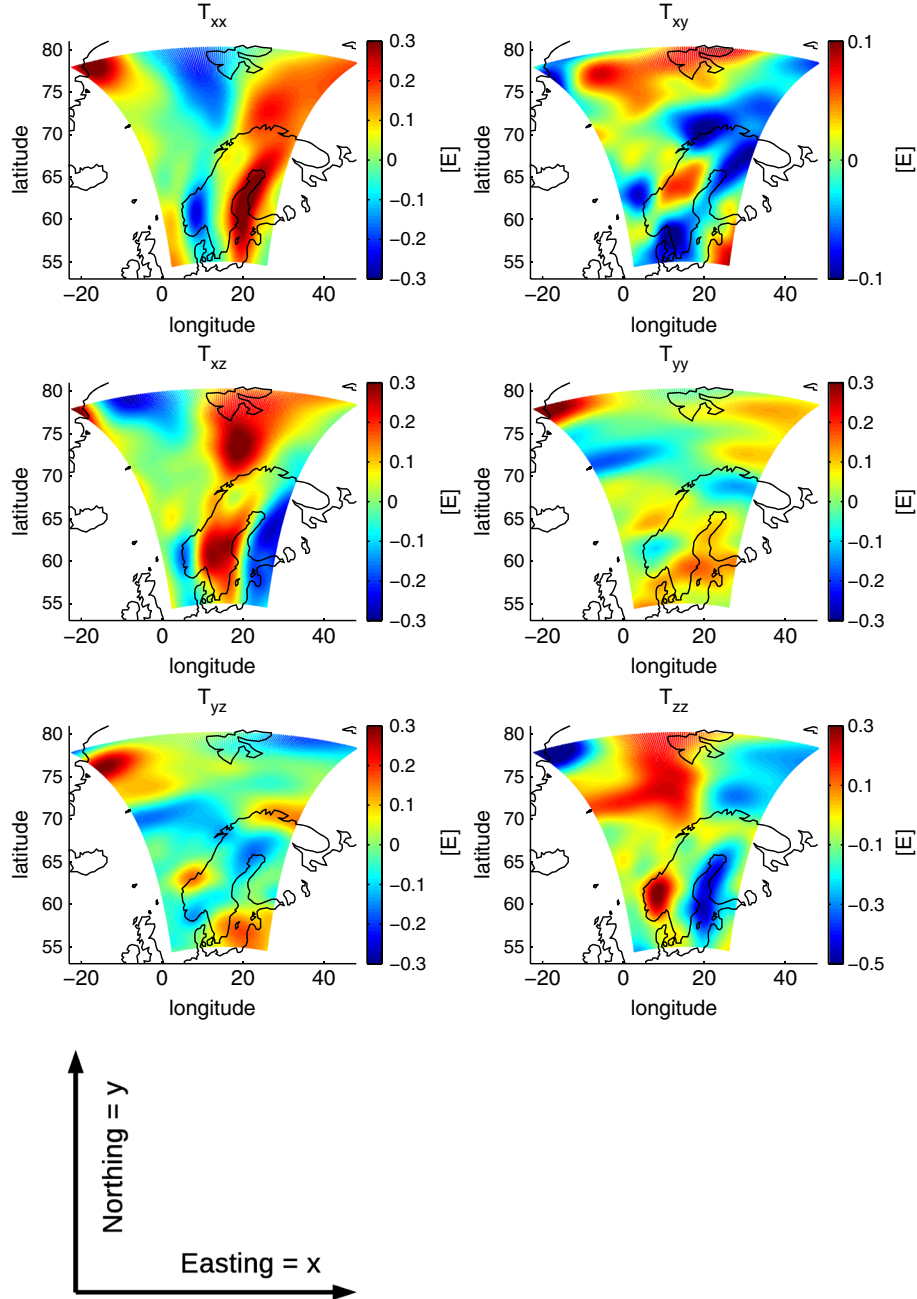


Figure 9. Gravity gradients in MRF at GOCE altitude computed from GOCO02S degree 10–250. Color scales have been saturated. Note that now x is easting and y is northing.

for airborne data, for example when these data are to be combined with GOCE data for regions such as the North East Atlantic margin.

4. Topographic Mass Reduction: Spherical Versus Planar Computations

[58] Here, we discuss the differences between a topographic mass reduction in a spherical and Cartesian planar Earth system. For conventional gravity data, conventionally a curvature correction is applied as a step in producing the Bouguer anomaly, which converts the geometry for the Bouguer correction from an infinite slab to a spherical cap

whose thickness is the elevation of the station and whose radius (arc length) from the station is 166.735 km, according to LaFehr [1991]. Gravity gradients are less affected by the regional mass distribution, but of course the satellite indicates that the spherical geometry is important.

[59] When GOCE gradients are to be used in lithospheric modeling one wants to subtract the signal related to topography as this masks the lithospheric signal. The topography is relatively well known and for the NEA region global and regional models are available [Amante and Eakins, 2009; Jakobsson et al., 2012]. Figure 14 shows the vertical gravity gradient signal due to topography computed using planar approximation using GM-SYS 3D [Popowski et al., 2009]. The gravity

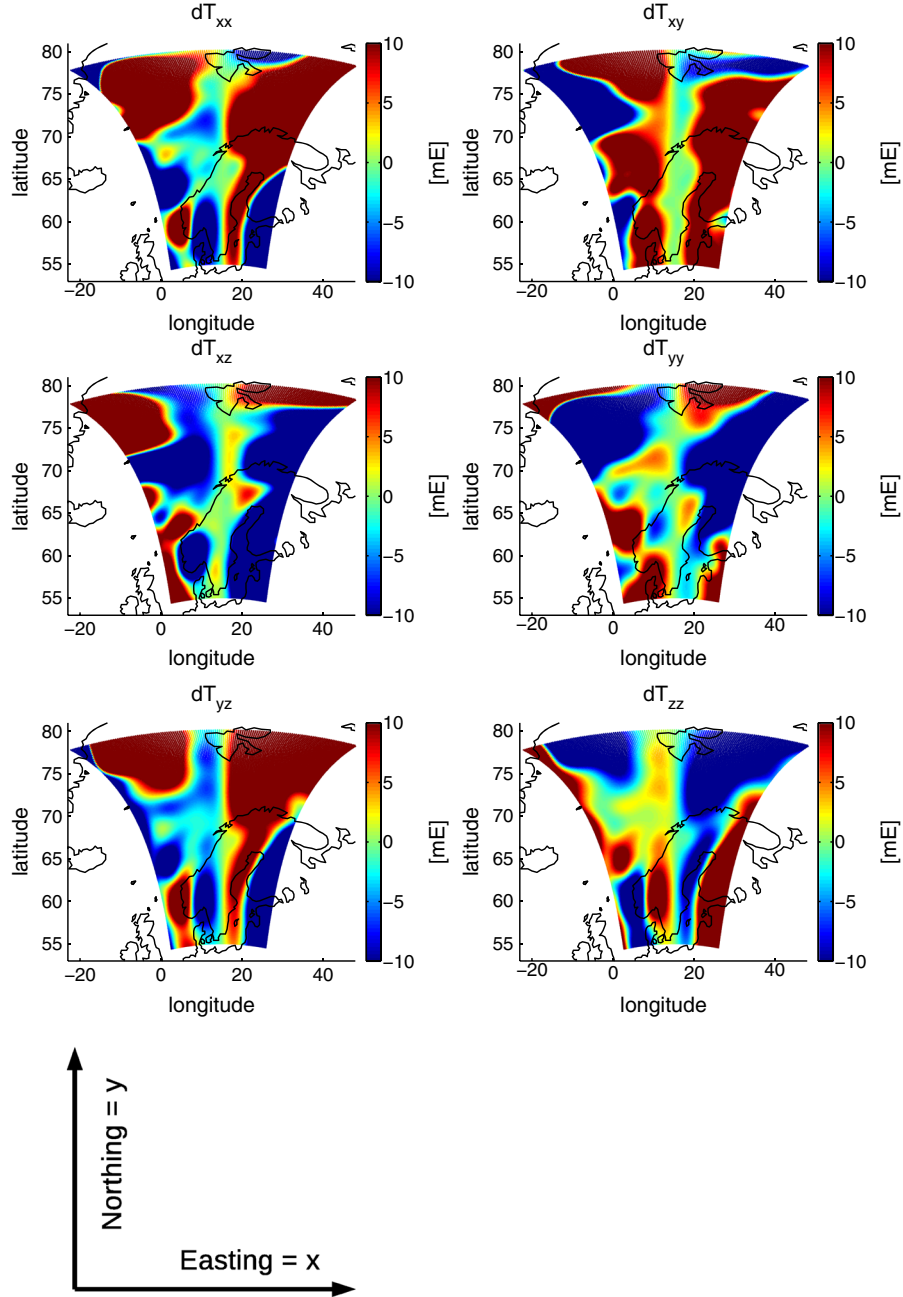


Figure 10. Difference between gradients in MRF using full rotations and gradients in MRF without corrections. Color scales have been saturated to ± 0.01 E.

gradients were calculated for a topographic model with 1 × 1 km resolution (Figure 14, left). The topographic mass reduction was calculated with a reduction density of 2670 kg/m^3 for the onshore topography and -1640 kg/m^3 for the water column (seawater density minus rock density).

[60] The top panel in Figure 15 shows the vertical gravity gradient signal at GOCE altitude due to topography from theETOPO1 model on a 1' grid using tesseroids [Uieda et al., 2011]. The topography model was chosen to be 5° larger than the computation area for the spherical computations, whereas in the planar case the topography is padded 100% to the sides. The bottom panel shows the differences with respect to the planar case where the difference in orientation

has been corrected using the rotations from MRF to LNOF discussed in section 3.2. The largest differences are in the lower left corner which are caused by edge effects in the planar computations, see Figure 14. In the planar computation

Table 2. Statistics of Gravity Gradient Differences in MRF @ 255 km Between Full Rotation and Accounting Only for Axes Differences. Units are [mE]

	T_{xx}	T_{xy}	T_{xz}	T_{yy}	T_{yz}	T_{zz}
Standard deviation	24.4	21.6	31.8	18.8	22.5	14.6
Maximum	98.4	70.0	237.7	64.2	126.4	86.4
Minimum	-131.9	-128.0	-79.0	-80.1	-209.5	-45.2

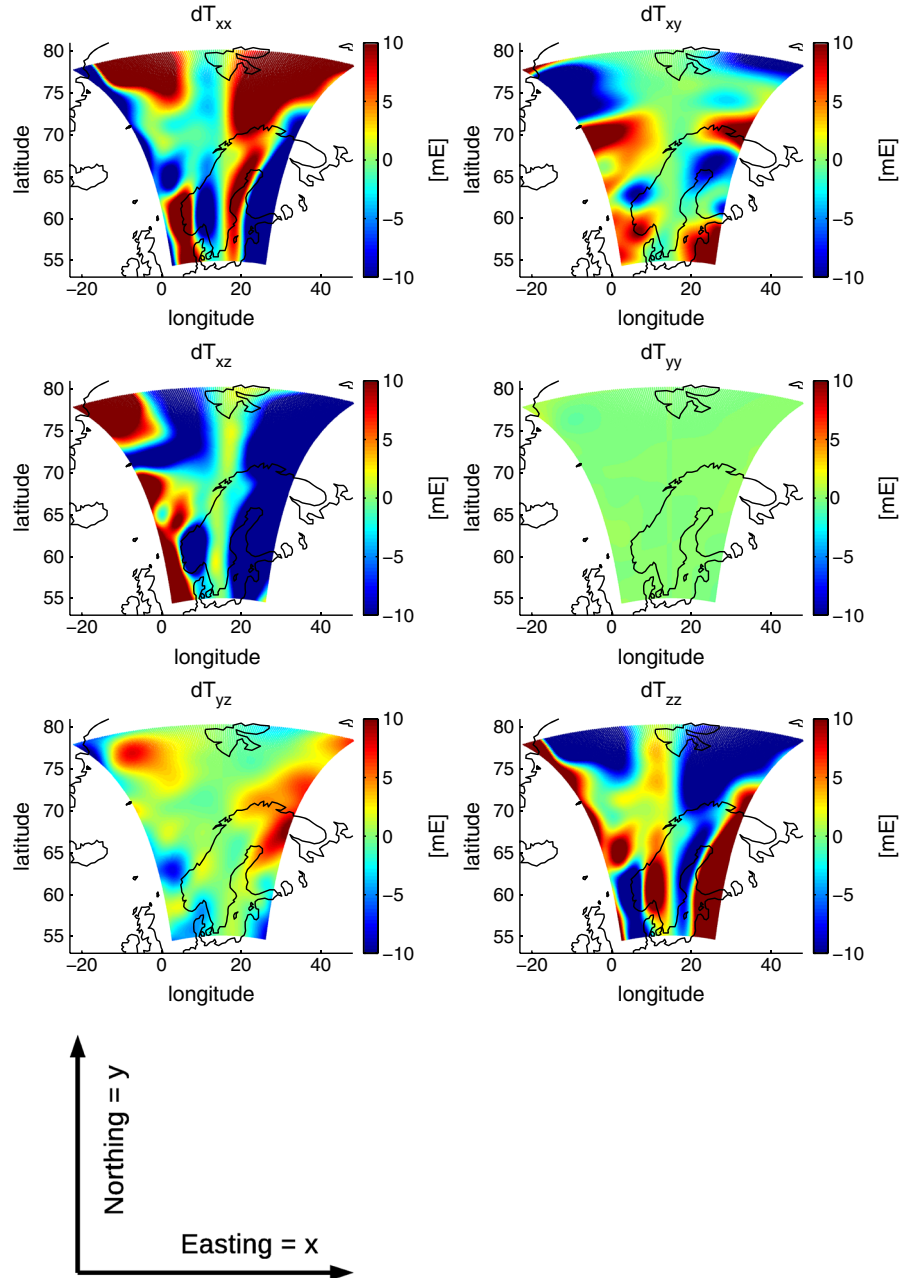


Figure 11. Gravity gradient differences in MRF between full rotation and accounting only for meridian convergence. Color scales have been saturated to ± 0.01 E.

the topography is mirrored outside the study area because data area and station locations have to be identical, which leads to such edge effects. Apart from these edge effects, there are long wavelength differences between the planar and spherical computations in the order of at least ± 0.5 E. We tested different resolutions of topography in both cases and also different padding/data extensions. While this affects the data at the border of the study area, it does not explain the overall difference between the calculations. The difference is caused by the source distance relation, which is only correct in the vertical direction for the planar case. All masses outside the vertical have an increased effect in the planar calculation than in the spherical calculation, as the distance between point of observation and mass point is

smaller than for a real spherical Earth. While this can be neglected for calculations within a small subset of the study area, such an error is significant on the regional scale and the GOCE satellite measurement bandwidth.

Table 3. Statistics of Gravity Gradient Differences in MRF @ 255 km Between Full Rotation and Accounting Only for Meridian Convergence. Units are [mE]

	T_{xx}	T_{xy}	T_{xz}	T_{yy}	T_{yz}	T_{zz}
Standard deviation	14.7	6.6	20.1	0.2	2.9	14.6
Maximum	45.1	22.6	11.6	1.4	11.2	86.4
Minimum	-86.9	-38.7	-51.3	-0.7	-12.3	-45.2

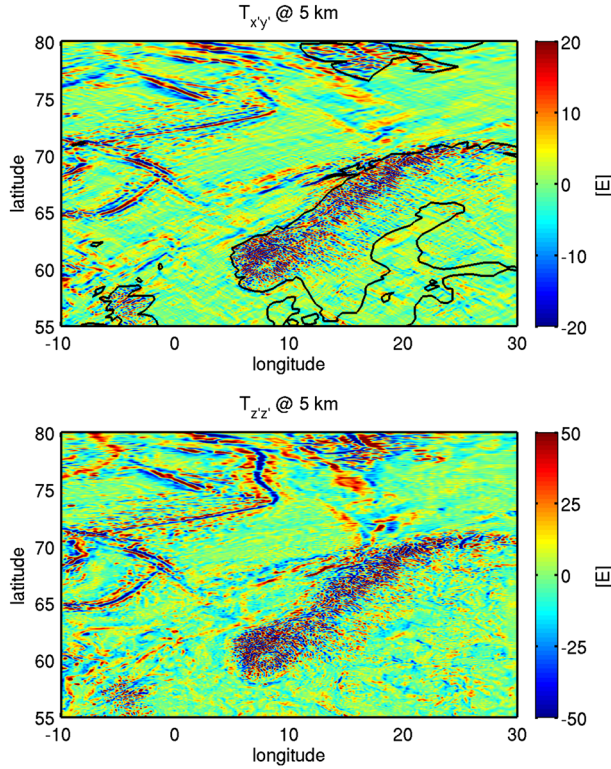


Figure 12. Gravity gradients in LNOF at 5 km altitude computed from EGM2008 degree 10–2190. Color scales have been saturated [E].

[61] Tables 7 and 8 show the statistics of topography gradient differences for all gradients before and after rotation to the MRF. The gradient differences in the lower left corner with $\lambda < 5^\circ$ and $\phi < 62^\circ$ are not considered. The mean differs from zero for almost all gradients and the maximum difference is up to 0.8 E. Rotation to the MRF reduces the standard deviation of the differences with 10–50% to 0.1–0.2 E, which is well above the errors caused by neglecting LNOF – MRF differences (Table 2). The conclusion therefore is that the differences in topographic gravity gradient signal are mainly caused by the planar approximation itself, not by the difference in orientation of the gradients.

[62] Another way to look at the differences between planar and spherical approximation is to consider gravity gradient tensor invariants. These are independent of the coordinate system, hence their name. Three invariants exist [Pedersen and Rasmussen, 1990]

$$\begin{aligned} I_0 &= \text{tr}(V_{ij}) = 0 \\ I_1 &= \frac{1}{2} \left((\text{tr } V_{ij})^2 - \text{tr}(V_{ij} V_{ij}) \right), \\ I_2 &= \det(V_{ij}) \end{aligned} \quad (11)$$

Table 4. Statistics of Gravity Gradient Signal in MRF @ 5 km. Units Are [E]

	T_{xx}	T_{xy}	T_{xz}	T_{yy}	T_{yz}	T_{zz}
Standard deviation	12.3	7.0	14.1	11.7	13.6	19.5
Maximum	154.7	90.9	187.5	170.0	197.6	342.3
Minimum	-170.6	-101.1	-186.8	-190.1	-193.8	-225.8

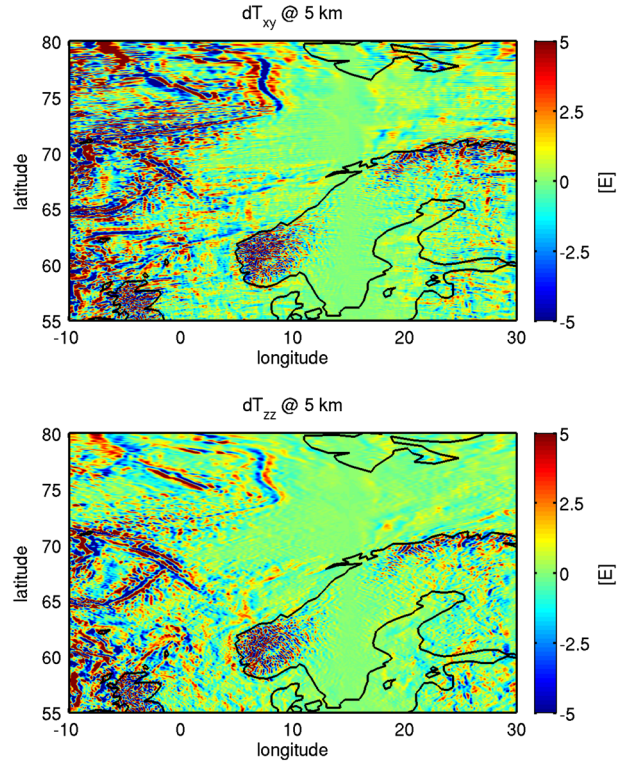


Figure 13. Difference between gradients in MRF using full rotations and gradients in MRF without corrections. Color scales have been saturated to ± 5 E.

with tr the trace, \det the determinant, and V_{ij} the gravity gradient tensor. As I_0 equals zero, we computed I_1 and I_2 for the gravity gradients from topography in planar and spherical approximation (see Figure 16). The invariants can directly be compared without performing a frame transformation. The amplitudes of the planar and spherical invariants differ and although the spatial patterns show similarities, significant differences occur. As before, we conclude that planar approximation may not be accurate enough and may lead to systematic errors in the computed gradients.

[63] We applied the topographic mass reduction to gravity gradients that were generated from the GOCO02S gravity field model from spherical harmonic degree $L = 10–250$. The topographic contribution from the tesseral computations was used, where the long wavelength contribution $L < 10$ has been subtracted using a spherical harmonic expansion of the topography based on DTM2006.0 [Grombein et al., 2012]. The reduced gradients are shown in Figure 17, where $x' = \text{west}$, $y' = \text{north}$, $z' = \text{up}$. The gradients reflect the lithospheric structure of the NE Atlantic [e.g., Ebbing et al.,

Table 5. Statistics of Gravity Gradient Differences in MRF @ 5 km Between Full Rotation and Accounting Only for Axes Differences. Units Are [E]

	T_{xx}	T_{xy}	T_{xz}	T_{yy}	T_{yz}	T_{zz}
Standard deviation	3.4	2.7	3.4	2.6	2.6	2.1
Relative to signal	28%	39%	24%	22%	19%	11%
Maximum	83.1	52.8	56.4	61.7	65.5	48.9
Minimum	-79.1	-68.5	-100.5	-66.1	-75.9	-45.3

Table 6. Relative Error in Gravity Gradients Accounting Only for Axes Differences Between LNOF and MRF @ 5 km. Signal Standard Deviation Is Compared With Error Standard Deviation Within a Maximum Longitude From the Central Meridian $\lambda = 15^\circ$

	T_{xx}	T_{xy}	T_{xz}	T_{yy}	T_{yz}	T_{zz}
$10^\circ < \lambda < 20^\circ$	6%	9%	5%	5%	5%	3%
$5^\circ < \lambda < 25^\circ$	13%	20%	12%	11%	10%	6%
$0^\circ < \lambda < 30^\circ$	17%	24%	15%	14%	12%	7%
$-10^\circ < \lambda < 30^\circ$	28%	39%	24%	22%	19%	11%

2012a] and would correspond to the Bouguer anomaly for the conventional gravity field. These gradients show both the signal associated with the transition from the oceanic plate to the continental shelf, and can for example be used to evaluate and improve crustal thickness compilations from seismic on a regional scale. Comparison with the Bouguer anomaly of the region shows already that the gradients are less affected than the Bouguer anomaly by regional trends from the deep lithosphere. The NE Atlantic gravity field has a dominating east-west trend, which cannot be explained by the lithosphere [see Ebbing and Olesen, 2005]. For gravity modeling, such a trend is often removed or explained by placing a small density contrast at the base lithosphere [e.g., Ebbing et al., 2012b]. The use of gravity gradients will potentially allow to verify such models and to verify regional trends associated with the deep lithosphere.

5. Conclusions and Discussion

[64] In geophysical modeling, commonly planar approximation is being used where the horizontal coordinates are

based on the UTM projection. On the other hand, airborne or satellite data are usually given in geographic or spherical coordinates. If gravity field quantities from lithospheric modeling are to be compared with these data, then one has to consider that not only is there a difference between map and geographic north, but also between the map normal and the normal to the ellipsoid or sphere. We derived the forward and inverse transformations between three-dimensional coordinates based on the UTM projection and geocentric coordinates. For a region in the North East Atlantic with an extension of $1500 \text{ km} \times 2800 \text{ km}$ we have shown that our transformations have an error below $1 \mu\text{m}$. Because the ellipsoidal and planar normal are different, a height above the ellipsoid is not exactly equal to a height above the plane. This difference, however, seems to lead to small gravity gradient errors at satellite altitude in our NEA test area and may be neglected.

[65] We also derived the exact relation between the three-dimensional UTM-based Cartesian system and the LNOF, which is a local Cartesian system that is defined with respect to spherical coordinates. The difference in orientation of the LNOF and the MRF may lead to gravity gradient errors that are large compared with the signal at satellite altitude and correcting only for meridian convergence is not sufficient. Also, in the case of airborne gradiometry these orientation differences may lead to significant systematic errors when larger areas are considered, e.g., when data from different airborne campaigns are merged with each other. Thus, in the combination of airborne and satellite data, and when using these data in lithospheric modeling, LNOF – MRF orientation differences should be accounted for.

[66] Proper lithospheric modeling requires topographic mass reduction as the topographic signal masks the

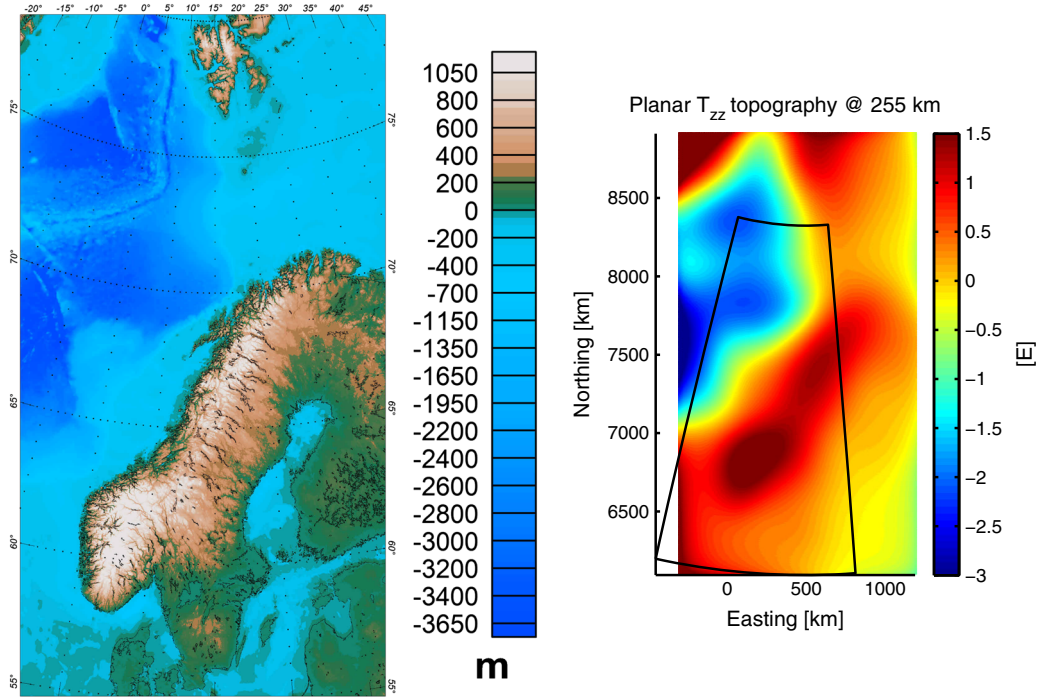


Figure 14. (left) Bathymetry and topography for the North East Atlantic margin. (right) Corresponding vertical gravity gradient signal at 255 km above the Earth's surface in planar approximation. Color scale has been saturated to the maximum and minimum of the spherical counterpart, which is computed in the black outlined area.

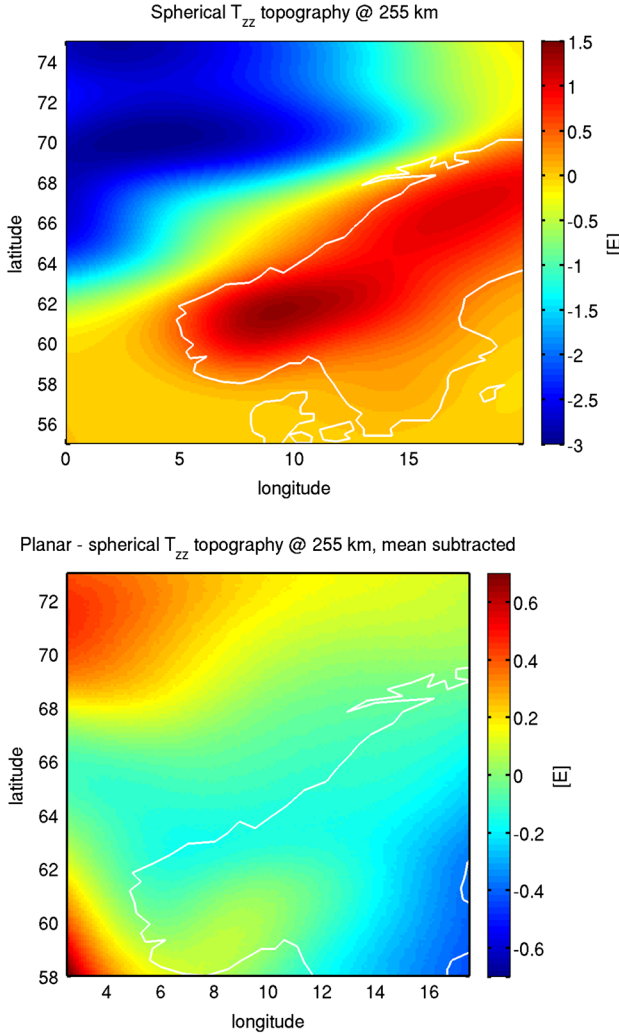


Figure 15. (top) Vertical gravity gradient signal at 255 km above the Earth's surface using tesseroids and (bottom) the differences with planar computations with the mean subtracted.

lithospheric signal. Similar to *Álvarez et al.* [2012], who demonstrated for a synthetic model the induced error by applying a planar instead of a spherical solution, we compared topography-induced gravity gradient signal at satellite altitude in planar and spherical approximation, where we accounted for the orientation differences of the reference frames. Long wavelength differences occur that are not negligible. Also a comparison of tensor invariants reveals such differences. This demonstrates that if the field is calculated

Table 7. Statistics of Gravity Gradient Differences [E] From Topographic Masses in Planar and Spherical Approximation Before Rotation @ 255 km

	T_{xx}	T_{xy}	T_{xz}	T_{yy}	T_{yz}	T_{zz}
Minimum	-0.02	-0.15	-0.18	-0.12	-0.21	-0.84
Maximum	0.80	0.32	0.54	0.32	0.25	0.03
Mean	0.38	-0.02	0.26	0.06	-0.05	-0.47
Standard deviation	0.19	0.09	0.12	0.08	0.10	0.19

Table 8. Statistics of Gravity Gradient Differences [E] From Topographic Masses in Planar and Spherical Approximation After Rotation @ 255 km

	T_{xx}	T_{xy}	T_{xz}	T_{yy}	T_{yz}	T_{zz}
Minimum	-0.05	-0.13	0.06	-0.09	-0.21	-0.79
Maximum	0.68	0.11	0.52	0.25	0.06	0.04
Mean	0.34	-0.04	0.27	0.07	-0.10	-0.43
Standard deviation	0.16	0.06	0.08	0.06	0.05	0.17

at satellite height, the mass sources must be presented in a spherical Earth frame. Otherwise, the mass sources outside the vertical cause long-wavelength effects due to the incorrect point-mass distances. Although gravity gradients are generally less affected by regional trends in the fields, one has to be careful not to generate such trends to be able to analyze the lithospheric density structure.

[67] On a regional scale and using satellite and/or airborne data we may conclude that at least the topographic mass reduction in planar approximation is not accurate enough, even when accounting for the reference frame differences. This also hints that the lithospheric modeling should be done in spherical approximation if satellite data are to be included. Our tool for tensor rotation between LNOF and MRF may become useful when for example airborne data from different campaigns and neighboring regions are to be combined with satellite data. On the other hand, the tool may be helpful for use on a local scale, when the use of a local system is justified and one wants to include satellite and/or airborne data in the model reference frame in a consistent manner, thus avoiding systematic errors that may result from reference frame differences.

[68] Finally, one problem in satellite and airborne gravimetry is that not all elements of the gravity gradient tensor are available or are available with very different accuracies [*Bouman et al.*, 2011b; *Dransfield and Lee*, 2004; *Fitzgerald*

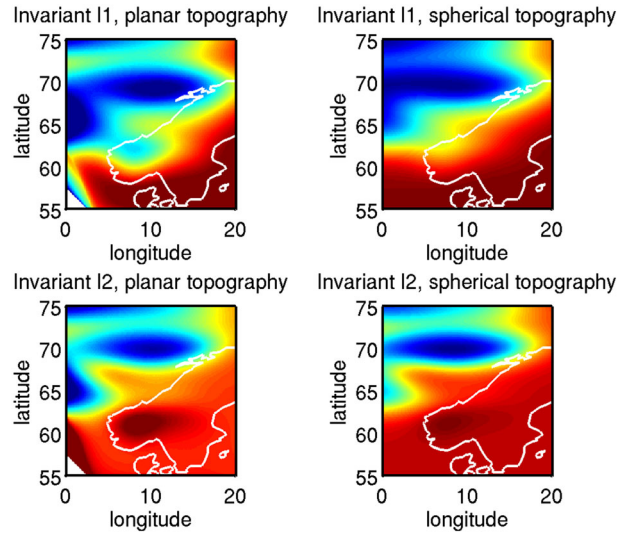


Figure 16. Invariants I1 and I2 computed from topography induced gravity gradient signal at 255 km altitude above the Earth's surface. (left) Planar case and (right) spherical case.

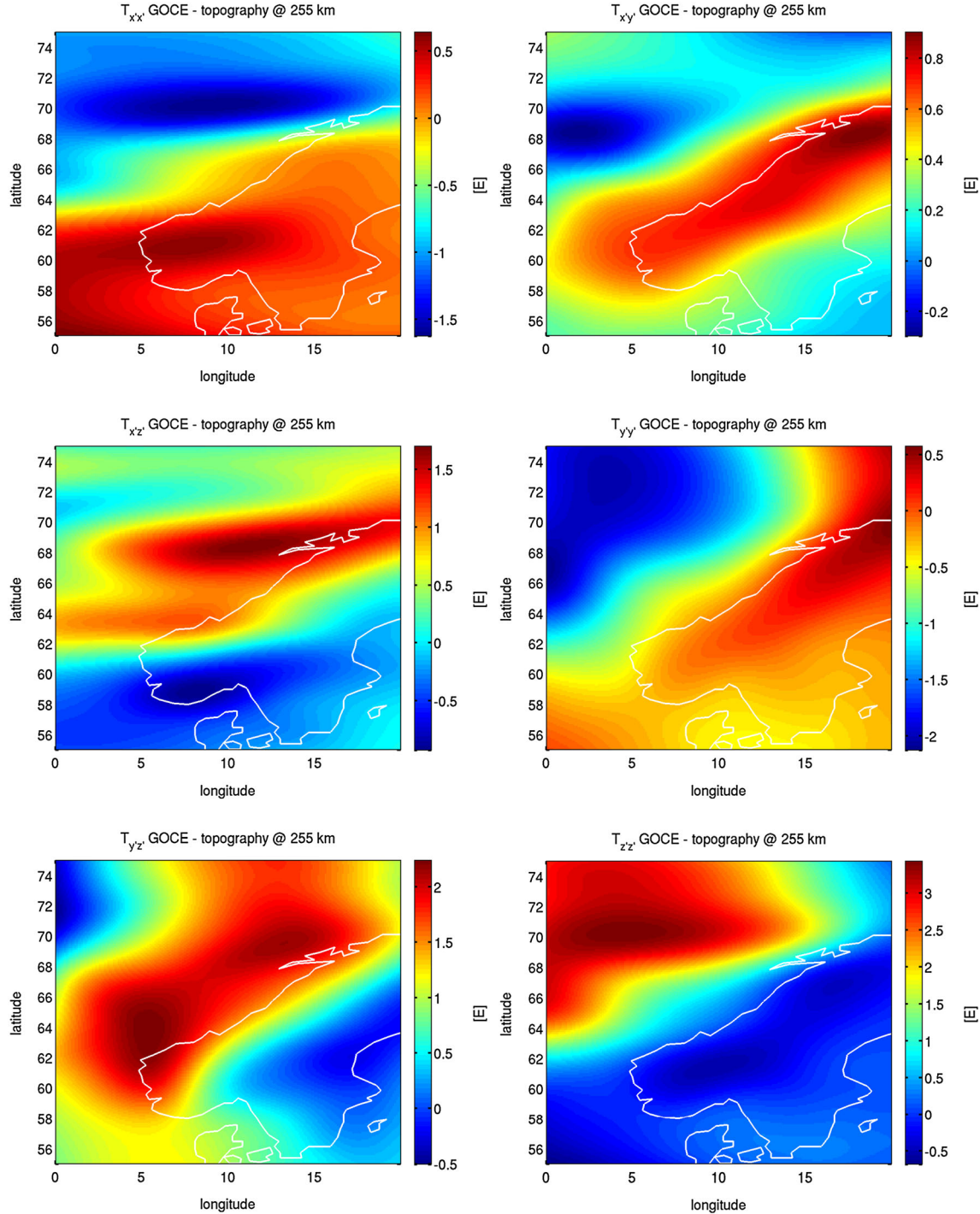


Figure 17. Gradients from GOCO02S ($L = 10\text{--}250$) reduced with topographic signal from tesseroidal computations (contribution $L < 10$ subtracted) @ 255 km altitude.

et al., 2012]. Fuchs and Bouman [2011] circumvent this problem for GOCE by introducing information from global gravity field models, with the potential disadvantage of biasing the rotated gradients towards the model. Fitzgerald et al. [2012] locally fit a potential function to the available airborne gradiometer data and then reestimate the gravity gradient tensor. In contrast to real measurements, all gravity gradients can directly be generated from a lithospheric

model and it is in principle possible to use only a subset of these to improve the lithospheric modeling. Limiting factor then is that lithospheric models are usually set up in planar approximation and gradients in rotated reference frame cannot be included. Consequently, improved lithospheric modeling should be able to deal with different reference frames to take full advantage of the available measured gradients.

Appendix A: Coordinate Transformations From Geocentric Cartesian to Spherical and Geographic Coordinates

[69] The transformation of spherical coordinates to geocentric Cartesian coordinates is given as

$$\begin{aligned} X &= r \cos \phi \cos \lambda \\ Y &= r \cos \phi \sin \lambda, \\ Z &= r \sin \phi \end{aligned} \quad (\text{A1})$$

and the transformation from geodetic coordinates to geocentric Cartesian coordinates is given as

$$\begin{aligned} X &= (N + h) \cos \varphi \cos \lambda \\ Y &= (N + h) \cos \varphi \sin \lambda, \\ Z &= (N(1 - e^2) + h) \sin \varphi \end{aligned} \quad (\text{A2})$$

with $N = a(1 - e^2 \sin^2 \varphi)^{\frac{1}{2}}$.

[70] The inverse transformations are given by

$$\begin{aligned} r &= \sqrt{X^2 + Y^2 + Z^2} \\ \lambda &= \text{atan} \frac{Y}{X}, \\ \phi &= \text{asin} \frac{Z}{r} \end{aligned} \quad (\text{A3})$$

and

$$\begin{aligned} \varphi &= \text{atan} \frac{Z + e^2 b \sin^3 \mu}{d - e^2 a \cos^3 \mu} \\ \lambda &= \text{atan} \frac{Y}{X}, \\ h &= \frac{d}{\cos \varphi} - N \end{aligned} \quad (\text{A4})$$

for spherical and geodetic coordinates, respectively, with

$$\begin{aligned} d &= \sqrt{X^2 + Y^2} \\ \mu &= \text{atan} \frac{Z a}{d b} \\ e'^2 &= \frac{a^2 - b^2}{b^2} = \frac{e^2}{1 - e^2} = \frac{2f - f^2}{(1 - f)^2}, \end{aligned} \quad (\text{A5})$$

see [Bowring, 1976; Strang van Hees, 2006].

A1. From Geodetic to UTM Coordinates

A1.1. From Geodetic Longitude and Latitude to Northing and Easting

[71] We follow Karney [2011] who based his equations on Krüger [1912]. UTM coordinates are computed with

$$\begin{aligned} N &= kA\xi + N_0 \\ E &= kA\eta + E_0 \end{aligned}$$

where false northing and easting are $N_0 = 500,000$ m and $E_0 = 0$ m, respectively, and the scale factor $k = 0.9996$ and

$$A = \frac{a}{1 + n} \left(1 + \frac{1}{4} n^2 + \frac{1}{64} n^4 \right), \quad (\text{A6})$$

with $2\pi A$ the circumference of a meridian and third flattening $n = f/(2 - f)$. The variables ξ and η are computed as

$$\begin{aligned} \xi &= \xi' + \sum_{j=1}^4 a_j \sin 2j\xi' \cosh 2j\eta' \\ \eta &= \eta' + \sum_{j=1}^4 a_j \cos 2j\xi' \sinh 2j\eta' \end{aligned} \quad (\text{A7})$$

where

$$\begin{aligned} a_1 &= \frac{1}{2}n - \frac{2}{3}n^2 + \frac{5}{16}n^3 + \frac{41}{180}n^4 \\ a_2 &= \frac{13}{48}n^2 - \frac{3}{5}n^3 + \frac{557}{1440}n^4 \\ a_3 &= \frac{61}{240}n^3 - \frac{103}{140}n^4 \\ a_4 &= \frac{49,561}{161,280}n^4 \end{aligned}, \quad (\text{A8})$$

and

$$\begin{aligned} \xi' &= \tan^{-1} \frac{\tau'}{\cos \lambda} \\ \eta' &= \sinh^{-1} \frac{\sin \lambda}{\sqrt{\tau'^2 + \cos^2 \lambda}} \end{aligned}, \quad (\text{A9})$$

with

$$\tau' = \tau \sqrt{1 + \sigma^2} - \sigma \sqrt{1 + \tau^2}, \quad (\text{A10})$$

where

$$\begin{aligned} \tau &= \tan \varphi \\ \sigma &= \sinh \left(e \tanh^{-1} \frac{e\tau}{\sqrt{1 + \tau^2}} \right). \end{aligned} \quad (\text{A11})$$

A1.2. From Northing and Easting to Geodetic Longitude and Latitude

[72] From the forward projection we have

$$\begin{aligned} \frac{N - N_0}{kA} &= \xi \\ \frac{E - E_0}{kA} &= \eta. \end{aligned} \quad (\text{A12})$$

[73] The variables ξ' and η' are computed as

$$\begin{aligned} \xi' &= \xi - \sum_{j=1}^4 \beta_j \sin 2j\xi' \cosh 2j\eta' \\ \eta' &= \eta - \sum_{j=1}^4 \beta_j \cos 2j\xi' \sinh 2j\eta', \end{aligned} \quad (\text{A13})$$

where

$$\begin{aligned} \beta_1 &= \frac{1}{2}n - \frac{2}{3}n^2 + \frac{37}{96}n^3 - \frac{1}{360}n^4 \\ \beta_2 &= \frac{1}{48}n^2 + \frac{1}{15}n^3 - \frac{437}{1440}n^4 \\ \beta_3 &= \frac{17}{480}n^3 - \frac{37}{840}n^4 \\ \beta_4 &= \frac{4397}{161,280}n^4. \end{aligned} \quad (\text{A14})$$

The geodetic longitude then is

$$\lambda = \tan^{-1} \frac{\sinh \eta'}{\cos \xi'}, \quad (\text{A15})$$

and the geodetic latitude is then obtained by Newton iteration using the initial value

$$\tau' = \frac{\sin \xi'}{\sqrt{\sinh^2 \eta' + \cos^2 \xi'}}, \quad (\text{A16})$$

in

$$\begin{aligned}\tau_i &= \begin{cases} \tau' & \text{for } i = 0 \\ \tau_{i-1} + \delta\tau_{i-1} & \text{otherwise,} \end{cases} \\ \tau'_i &= \tau_i \sqrt{1 + \sigma_i^2} - \sigma_i \sqrt{1 + \tau_i^2} \\ \delta\tau_i &= \frac{\tau' - \tau'_i}{\sqrt{1 + \tau_i^2}} \frac{1 + (1 - e^2)\tau_i^2}{(1 - e^2)\sqrt{1 + \tau_i^2}}.\end{aligned}\quad (\text{A17})$$

[74] The geodetic latitude now is

$$\varphi = \tan^{-1}\tau. \quad (\text{A18})$$

[75] **Acknowledgments.** This work has been done in the framework of the ESA sponsored GOCE+GeoExplore study as part of ESA's Support to Science Element. The constructive comments by two referees helped to improve the paper.

References

- Álvarez, O., M. Giménez, C. Braatenberg, and A. Folguera (2012), GOCE satellite derived gravity and gravity gradient corrected for topographic effect in the South Central Andes region, *Geophys. J. Int.*, doi:10.1111/j.1365-246X.2012.05556.x.
- Amante, C., and B. W. Eakins (2009), ETOPO1 1 Arc-Minute Global Relief Model: Procedures, Data Sources and Analysis, *NOAA Technical Memorandum NESDIS NGDC-24*, 19 pp, March 2009.
- Barrère, C., J. Ebbing, and L. Gernigon (2011), 3D density and magnetic crustal characterisation of the southwestern Barents Shelf: implications for the offshore prolongation of the Norwegian Caledonides, *Geophys. J. Int.*, doi:10.1111/j.1365-246X.2010.04888.x.
- Bouman, J., S. Rispen, T. Gruber, R. Koop, E. Schrama, P. Visser, C. C. Tscherning, and M. Veichert (2009), Preprocessing of gravity gradients at the GOCE high-level processing facility, *J. of Geod.*, 83, 659–678.
- Bouman, J., J. Ebbing, M. Fuchs, M. Schmidt, W. Bosch, C. Schwatke, R. Abdul Fattah, S. Meekes, O. Abbink, Y. Schavemaker (2011a), Heterogeneous gravity data combination for Earth interior and geophysical exploration research, in *Proceedings GOCE User Workshop 2011*, ESA SP-696.
- Bouman, J., S. Fiorot, M. Fuchs, T. Gruber, E. Schrama, C. C. Tscherning, M. Veichert, and P. Visser (2011b), GOCE Gravitational Gradients along the Orbit, *J. of Geod.*, 85, 791–805, doi:10.1007/s00190-011-0464-0.
- Bowin, C. (1991), The Earth's gravity field and plate tectonics, *Tectonophysics*, 187, 69–89.
- Bowring, B. R. (1976), Transformation from spatial to geographical coordinates, *Survey Review*, 181, July, 323–327.
- Braatenberg, C., M. Sprlak, P. Mariani, and J. Ebbing (2011), The global gravity Marussi tensor and the enigmatic Chad lineament, in *The Formation and Evolution of Africa: A Synopsis of 3.8 Ga of Earth History*, edited by D. J. J. Van Hinsbergen et al., Geological Society, London, Special Publications, 357, 329–341, doi:10.1144/SP357.18.
- Dransfield, M. H., and J. B. Lee (2004), The FALCON airborne gravity gradiometer survey systems, edited by R. Lane, *Airborne Gravity 2004 - Abstracts from the ASEG-PESA Airborne Gravity 2004 Workshop*, *Geoscience Australia Record 2004/18*, 15–19.
- Ebbing, J., and O. Olesen (2005), The Northern and Southern Scandes – Structural differences revealed by an analysis of gravity anomalies, the geoid and regional isostasy, *Tectonophysics*, 411, 73–87.
- Ebbing, J., J. Bouman, H. J. Götze, R. Haagmans, M. Fuchs, S. Meekes, and R. Abdul Fattah (2012a), Use of GOCE satellite gradient gravity data for forward and inverse modeling of the NE Atlantic margin, paper presented at 74th EAGE Conference and Exhibition, Copenhagen, June 2012a.
- Ebbing, J., R. W. England, T. Korja, T. Lauritsen, O. Olesen, W. Stratford, and C. Weidle (2012b), Structure of the Scandes lithosphere from surface to depth, *Tectonophysics*, doi:10.1016/j.tecto.2011.03.031.
- Fitzgerald, D. J., R. Paterson, and H. Holstein (2012), Comparing two methods for gridding and honouring gravity gradient tensor data, paper presented at 74th EAGE Conference and Exhibition, Copenhagen, June 2012.
- Fuchs, M., and J. Bouman (2011), Rotation of GOCE gravity gradients to local frames, *Geophys. J. Int.*, 187, 743–753, doi:10.1111/j.1365-246X.2011.05162.x.
- Goiginger, H., et al. (2011), The combined satellite-only global gravity field model GOCO02S, paper presented at the 2011 General Assembly of the European Geosciences Union, Vienna, Austria, April 4–8.
- Grombein, T., K. Seitz, and B. Heck (2012), Topographic-isostatic reduction of GOCE gravity gradients, in *Proceedings of the XXV General Assembly of the International Union of Geodesy and Geophysics*, Melbourne, Australia. International Association of Geodesy Symposia, Vol. 139, Springer (accepted).
- Gruber, T., R. Rummel, O. Abrikosov, and R. van Hees (2010), GOCE level 2 product data handbook, *GO-MA-HPF-GS-0110*, issue 4.2.
- Hirt, C., M. Kuhn, W. E. Featherstone, and F. Göttl (2012), Topographic/ isostatic evaluation of new-generation GOCE gravity field models, *J. Geophys. Res.*, 117, B05407, doi:10.1029/2011JB008878.
- Jakobsson, M., et al. (2012), The International Bathymetric Chart of the Arctic Ocean (IBCAO) Version 3.0, *Geophys. Res. Lett.*, doi:10.1029/2012GL052219, in press.
- Karney, C. F. F. (2011), Transverse Mercator with an accuracy of a few nanometers, *J. of Geod.*, 85, 475–485, doi:10.1007/s00190-011-0445-3.
- Krüger, J. H. L. (1912), Konforme Abbildung des Erdellipsoide in der Ebene, *New Series* 52, Royal Prussian Geodetic Institute, Potsdam, doi:10.2312/GFZ.b103-krueger28.
- LaFehr, T. R. (1991), An exact solution for the gravity curvature (Bullard B) correction, *Geophysics*, 56, 1179–1184.
- Pavlis, N. K., S. A. Holmes, S. C. Kenyon, and J. K. Factor (2012), The development and evaluation of the Earth Gravitational Model 2008 (EGM2008), *J. Geophys. Res.*, 117, B4, doi:10.1029/2011JB008916.
- Pedersen, L. B., and T. M. Rasmussen (1990), The gradient tensor of potential anomalies: Some implications on data collection and data processing maps, *Geophysics*, 55, 1558–1566, doi:10.1190/1.1442807.
- Popowski, T., G. Connard, R. French (2009), GM-SYS profile modeling, Gravity and Magnetic Modeling software for OasisMontaj – *User Guide*, v 4.1, Northwest Geophysical Associates, Corvallis, Oregon.
- Strang van Hees, G. (2006), Globale en lokale geodetische systemen, *Publikatie 30*, 2nd ed., Nederlandse Commissie voor Geodesie, Delft.
- Tašárová, Z., H. J. Götze, R. El-Kelani, J. Ebbing, M. Hassouneh, and DESERT Group (2006), Small-scale gravity modeling of upper crustal structures in the Arava Valley along the Dead Sea Transform, *G3*, 7(9), doi:10.1029/2005GC001229.
- Torge, W. (2001), *Geodesy*, de Gruyter, Berlin, New York.
- Uieda, L., E. Bomfim, C. Braatenberg, and E. Molina (2011), Optimal forward calculation method of the Marussi tensor due to a geologic structure at GOCE height, in *Proceedings GOCE User Workshop 2011*, ESA SP-696.
- Zeyen, H., M. Fernández (1994), Integrated lithospheric modeling combining thermal, gravity, and local isostasy analysis: Application to the NE Spanish Geotransect, *J. Geophys. Res.*, 99, 18,089–18,102.